Expedite your small-field dosimetry workflow.

SRS MapCHECK™

SRS PATIENT QA, NO FILM

See it firsthand at AAPM 2018

Learn More

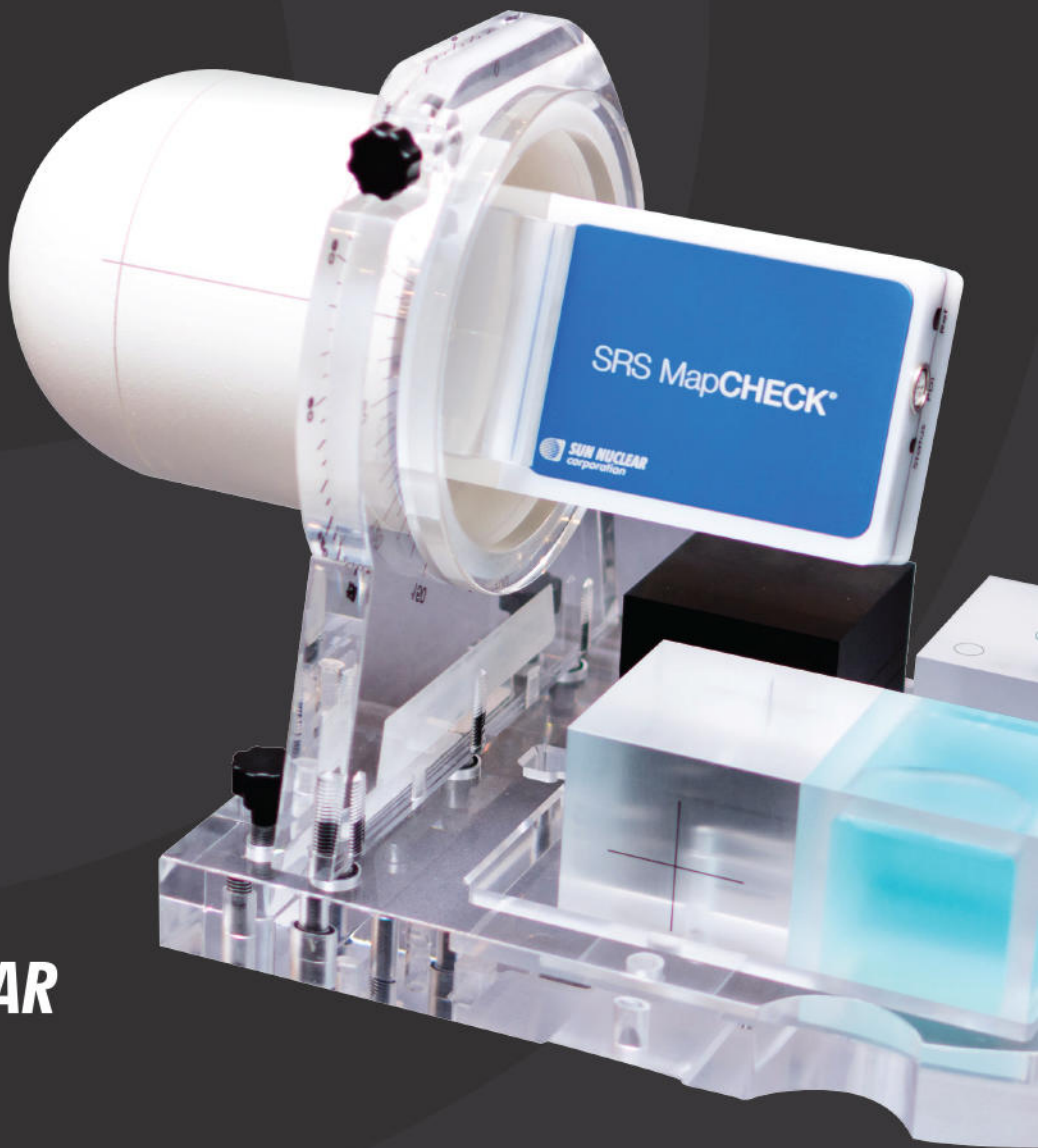

SUN NUCLEAR corporation

Impact of interpatient variability on organ dose estimates according to MIRD schema: Uncertainty and variance-based sensitivity analysis

Alexandra Zvereva[a)]
Institute of Radiation Protection, Helmholtz Zentrum München, German Research Center for Environmental Health, Neuherberg 85764, Germany
Department of Medical Physics, Ludwig-Maximilians-Universität München (LMU Munich), Garching 85748, Germany

Florian Kamp
Department of Radiation Oncology, University Hospital, LMU Munich, Munich 81377, Germany

Helmut Schlattl, and Maria Zankl
Institute of Radiation Protection, Helmholtz Zentrum München, German Research Center for Environmental Health, Neuherberg 85764, Germany

Katia Parodi
Department of Medical Physics, Ludwig-Maximilians-Universität München (LMU Munich), Garching 85748, Germany

(Received 19 October 2017; revised 1 May 2018; accepted for publication 8 May 2018; published xx xxxx xxxx)

Purpose: Variance-based sensitivity analysis (SA) is described and applied to the radiation dosimetry model proposed by the Committee on Medical Internal Radiation Dose (MIRD) for the organ-level absorbed dose calculations in nuclear medicine. The uncertainties in the dose coefficients thus calculated are also evaluated.

Methods: A Monte Carlo approach was used to compute first-order and total-effect SA indices, which rank the input factors according to their influence on the uncertainty in the output organ doses. These methods were applied to the radiopharmaceutical (S)-4-(3-^{18}F-fluoropropyl)-L-glutamic acid (^{18}F-FSPG) as an example. Since ^{18}F-FSPG has 11 notable source regions, a 22-dimensional model was considered here, where 11 input factors are the time-integrated activity coefficients (TIACs) in the source regions and 11 input factors correspond to the sets of the specific absorbed fractions (SAFs) employed in the dose calculation. The SA was restricted to the foregoing 22 input factors. The distributions of the input factors were built based on TIACs of five individuals to whom the radiopharmaceutical ^{18}F-FSPG was administered and six anatomical models, representing two reference, two overweight, and two slim individuals. The self-absorption SAFs were mass-scaled to correspond to the reference organ masses.

Results: The estimated relative uncertainties were in the range 10%–30%, with a minimum and a maximum for absorbed dose coefficients for urinary bladder wall and heart wall, respectively. The applied global variance-based SA enabled us to identify the input factors that have the highest influence on the uncertainty in the organ doses. With the applied mass-scaling of the self-absorption SAFs, these factors included the TIACs for absorbed dose coefficients in the source regions and the SAFs from blood as source region for absorbed dose coefficients in highly vascularized target regions. For some combinations of proximal target and source regions, the corresponding cross-fire SAFs were found to have an impact.

Conclusion: Global variance-based SA has been for the first time applied to the MIRD schema for internal dose calculation. Our findings suggest that uncertainties in computed organ doses can be substantially reduced by performing an accurate determination of TIACs in the source regions, accompanied by the estimation of individual source region masses along with the usage of an appropriate blood distribution in a patient's body and, in a few cases, the cross-fire SAFs from proximal source regions. [https://doi.org/10.1002/mp.12984]

Key words: global sensitivity analysis, internal dose, PET, uncertainty analysis

1. INTRODUCTION

The standard method of organ-level absorbed dose calculation in nuclear medicine is described in the pamphlet 21 of the Committee on Medical Internal Radiation Dose (MIRD).[1] It relies on the knowledge of the spatial and temporal distribution of an injected radiopharmaceutical in the patient's body and the specific absorbed fractions (SAFs). The former is characterized by time-integrated activity coefficients (TIACs) which are necessary input quantities in the MIRD schema. The option for obtaining such data is direct patient imaging and quantification or pharmacokinetic

modeling. SAFs are usually derived by Monte Carlo calculations in the geometry of the human body. The latter is either represented by patient computed tomography (CT) image sets or simulated by a generic anatomical model.

Stabin,[2] Flux et al.,[3] and Mattsson[4] pointed out the benefit to the patient of individualized dosimetry in nuclear medicine. Individualized dosimetry according to the MIRD schema requires the estimation of individual TIACs and the computation of SAFs based on patient-specific anatomical data. However, the collection of patient data required for the calculation of individual TIACs is often not done in routine clinical practice. Moreover, despite the rapid spread of hybrid nuclear medicine imaging devices integrating CT scanners, organ segmentation in individual CT image sets is likewise not usually done. Consequently, such individual data are often approximated by reference TIACs and reference anatomy. This approach is prone to considerable uncertainties. There is a need to quantify uncertainties in computed doses in applications such as toxicology, pharmacology, medicine,[5] or in epidemiological studies.[6] It is also of interest to study ways to enhance the accuracy of internal dose estimates.

Paquet et al.[5] and Stabin[7] summarized the main sources of uncertainties associated with internal dosimetry. Stabin[7] stated that the total uncertainty can amount to a factor of 2 or more. Spielmann et al.[8] quantified uncertainties in computed organ doses for seven radiopharmaceuticals. Besides the uncertainty analysis reported so far by different authors, a key procedure used to assess the quality of a model-based study is sensitivity analysis (SA).[9] This is an evaluation of the relative importance of different input factors on the model output. SA may yield the following practically important results: first, identifying those input factors that have a large influence on the uncertainty in the model output, therefore indicating an efficient way to decrease the overall uncertainty; and second, fixing those input factors that do not affect the model output over their realistic range of variation, thus reducing the model complexity. Saltelli et al.[10] denoted the foregoing considerations as "factor prioritization" and "factor fixing", respectively. For the sake of simplicity, we refer to the calculation of organ absorbed dose coefficients as the "model" and the dose coefficients thus computed as the "model output".

Ferretti et al.[11] showed that the majority of published papers use "one-factor-at-a-time" (OAT) SA approach. This strategy evaluates the effect on the model output of the change of one variable input at a time around a selected point (often the mean value), while keeping all other inputs constant. This approach neglects any interaction among the input parameters. Additionally, with OAT the input space is not fully interrogated. This effect becomes more severe with the increase of the number of input parameters ("curse of dimensionality").[9] In contrast to OAT, global variance-based techniques[12–14] are effective and do not require the assumptions of linearity and additivity of a model. Additionally, the SA procedures, described in Ref. [10 and 14] for example, intrinsically include the uncertainty analysis and, hence, provide both uncertainty and sensitivity of the model output at once. In some works,[15] SA was used for pharmacokinetic models only. There has been little application of a global variance-based SA to organ dose estimation according to the MIRD schema.

The objective of this work was to quantify the uncertainties in the internal organ dose coefficients, when calculated in accordance with the MIRD formalism.[1] Two sources of uncertainty are considered: interindividual variability in TIACs and interphantom variability in SAFs. We aim at identifying the most influential inputs among the sets of TIACs and SAFs for the uncertainty in the computed output doses via the application of variance-based SA techniques.[14] As an example study, we applied these methods to the radiopharmaceutical (S)-4-(3-^{18}F-fluoropropyl)-L-glutamic acid (^{18}F-FSPG).

2. MATERIALS AND METHODS

2.A. Considered model for organ absorbed dose estimation

In this work, we examined the standard model of organ absorbed dose computation, described by Bolch et al.[1] According to it, the absorbed dose coefficient $d(r_T)$ in the target region r_T is calculated as:

$$d(r_T) = \sum_{r_S} TIAC(r_S) \cdot S(r_T \leftarrow r_S) + TIAC(r_{RoB}) \left(\frac{M_{TB} \cdot S(r_T \leftarrow r_{TB}) - \sum_{r_S} M_{r_S} \cdot S(r_T \leftarrow r_S)}{M_{TB} \sum_{r_S} M_{r_S}} \right) \quad (1)$$

with

$$S(r_T \leftarrow r_S) = \begin{cases} \int_0^{E_0} P(E) \cdot E \cdot SAF(r_T \leftarrow r_S, E) dE, & \text{for continuous emission spectra (β-spectrum)} \\ \sum_i E_i \cdot y_i \cdot SAF(r_T \leftarrow r_S, E_i), & \text{for discrete emission lines (photons)} \end{cases} \quad (2)$$

In Eqs. (1) and (2) r_{RoB} and r_S denote source region rest of body and other source regions, respectively. r_{RoB} is equal to the total body r_{TB} excluding all other source organs and tissues r_S. M_{TB} and M_{r_S} are masses of r_{TB} and r_S, respectively; E_i and y_i are mean energy and yield of radiation i, respectively; E and E_0 are energy and maximum energy of the β-spectrum, respectively. $P(E)$ is the number of β-particles emitted at energy E per MeV per nuclear transformation.

TIAC(r_S) and TIAC(r_{RoB}) denote TIACs for r_S and r_{RoB}, respectively. $SAF(r_T \leftarrow r_S, \mathrm{E})$ are SAFs for energy E, emitted in region r_S and absorbed in r_T.

A fixed urinary bladder model for the reference bladder content volume of 200 ml was used to compute the absorbed dose coefficients to urinary bladder wall. As can be seen from Eqs. (1) and (2), the input factors for the model include TIAC(r_S) and TIAC(r_{RoB}), the terms $S(r_T \leftarrow r_S)$ and $S(r_T \leftarrow r_{TB})$ for all combinations of r_T and r_S and all considered radiation types, E_i and y_i for each radiation i, as well as masses M_{TB} and M_{r_S}. The latter values were taken from the corresponding masses of the employed human computational phantom (see Section 2.D.). We assumed E_i, y_i and β-spectrum of the considered radiation types to be constant. Thus, the variable input parameters of the model comprised the TIACs and the SAFs. For the sake of convenience, we denote them as TIAC input factors and SAF input factors.

For the output Y (where the number of outputs Y is equal to the number of considered r_T) we can write:

$$Y = f(TIAC_1, TIAC_2, \ldots, TIAC_i, \ldots, TIAC_k, SAF_1, SAF_2, \ldots, SAF_i, \ldots, SAF_k) \tag{3}$$

with the model f defined by Eqs. (1) and (2) and the number of independent input factors being equal to $2k$, where k is the number of source regions. The model f was implemented in an in-house MATLAB-based (MATLAB, version 8.0.0.783 (R2012b), The MathWorks, Inc., Natick Massachusetts, 2012) program, which utilizes discrete photon energies and detailed β-spectra from Publication 107[16] of the International Commission on Radiological Protection (ICRP). This program includes the option of mass-scaling of the SAFs, first proposed in the MIRD Pamphlet 11[17] for the whole-body anatomical models and described elsewhere[18] for whole-body and partial-body phantoms. In this work, we also computed values denoted in the following as "weighted dose coefficients". They were calculated as a weighted sum of individual organ absorbed dose coefficients times their tissue weighting factors given in ICRP Publication 103.[19] The main difference between the weighted dose coefficients computed here and the effective dose coefficients defined by ICRP[19] is that the weighted dose coefficients are not sex- and age-averaged. Moreover, we excluded the following organs and tissues from their calculation: endosteum, lymphatic nodes, oral mucosa, muscle tissue, uterus, and prostate. All these regions were excluded because they were not present in at least one of the considered phantoms. In our SA study, we assumed the employed tissue weighting factors to be constant.

2.B. Variance-based sensitivity analysis

The variance-based SA techniques were implemented according to the development of Saltelli et al.[14] for first-order (or main) effect indices and of Jansen[20] and Saltelli et al.[14] for total-effect indices based on the work of Sobol'.[12]

Using the same nomenclature as in Eq. (3) for a model $Y = f(X_1,X_2,\ldots, X_i,\ldots,X_n)$ with n independent input factors ($n = 2k$ in Eq. 3), the first-order effect sensitivity index for the input factor X_i is defined as:

$$S_i = \frac{V_{X_i}(E_{X_{\sim i}}(Y|X_i - x_i^*))}{V(Y)} \tag{4}$$

In Eq. (4) the conditional expression $Y|X_i = x_i^*$ means the value of the model Y if the input X_i is fixed to a value x_i^*. $X_{\sim i}$ denotes the set of all input factors except X_i. $E_{X_{\sim i}}(Y|X_i - x_i^*)$ represents the mean value of the model Y for fixed $X_i = x_i^*$ but all other inputs $X_{j\neq i}$ varied. The numerator in Eq. (4) is the variance of $E_{X_{\sim i}}(Y|X_i - x_i^*)$ when varying all possible points x_i^*. The denominator $V(Y)$ is the total unconditional variance of the output.

The total-effect sensitivity index S_{T_i} for the input factor X_i includes the first-order effect and all the interactions of X_i.[21,22] Thus the fraction of output variance caused by $X_{\sim i}$ alone, that is the first-order effect sensitivity index for $X_{\sim i}$, needs to be excluded. According to these considerations and the law of total variance, S_{T_i} is given by

$$\begin{aligned} S_{T_i} &= 1 - \frac{V_{X_{\sim i}}(E_{X_i}(Y|X_{\sim i} = x^*_{\sim i}))}{V(Y)} \\ &= \frac{E_{X_{\sim i}}(V_{X_i}(Y|X_{\sim i} = x^*_{\sim i}))}{V(Y)}, \end{aligned} \tag{5}$$

where $\frac{V_{X_{\sim i}}(E_{X_i}(Y|X_{\sim i}))}{V(Y)}$ can be considered as S_i for $X_{\sim i}$ (Eq. 4). $V_{X_i}(Y|X_{\sim i} = x^*_{\sim i})$ is the variance over possible $X_i = x_i^*$ of the model Y, while keeping all input factors but X_i fixed. $E_{X_{\sim i}}(\ldots)$ is the mean of the argument taken over $X_{\sim i}$.

Both S_i and S_{T_i} can have values in the range [0, 1], where the importance of the corresponding input factor increases with increasing values of the SA index. For example, $S_i = 0$ and $S_{T_i} = 0$ mean, respectively, no main effect influence and no influence of the corresponding input factor on the model output. $S_i = 1$ means that the uncertainty in the output is solely caused by the variability of the input X_i. Pursuant to the definition, $S_{T_i} \geq S_i$, since the total-effect index includes main effect and all interactions of X_i.

In this work, a Monte Carlo technique was used to evaluate uncertainty and sensitivity of a model. According to this technique, all variable input factors are simultaneously sampled from their assigned distributions, providing a vector of input factors $(X_1,X_2,\ldots,X_i,\ldots,X_{2k})_1$. The model output is calculated with the vector of input factors $(X_1,X_2,\ldots,X_i,\ldots,X_{2k})_1$ and denoted as $f(X_1,X_2,\ldots,X_i,\ldots,X_{2k})_1$. This procedure is repeated N times, giving a matrix A of input factors with a size $N \times 2k$, where the j-th row represents the j-th sample of the input factors $(X_1,X_2,\ldots,X_i,\ldots,X_{2k})_j$. The model is executed for each sample of the inputs, providing a vector of outputs $Y = f(A)$ of length N. The variability of the output Y can be thus evaluated:

$$\sigma_Y = \sqrt{V(Y)} \tag{6}$$

The relative uncertainty is computed as:

$$RU = \frac{\sigma_Y}{E(Y)} \tag{7}$$

The generated samples of inputs and the corresponding model outputs are used for the SA. Saltelli et al.[14] proposed the following approach to compute S_i:

$$S_i = \frac{\frac{1}{N}\sum_{j=1}^{N} f(B)_j \left(f\left(A_B^{(i)}\right)_j - f(A)_j \right)}{V(Y)} \quad (8)$$

where N is the number of model evaluations. A and B are independent sampled matrices of input factors with a size of $N \times 2k$, generated as described above for the example of matrix A. $A_B^{(i)}$ is equal to the matrix A, except for the column i, which is taken from the matrix B, thus X_i = const (see Eq. (4)). $(A)_j$ and $(B)_j$ are the j-th rows of A and B, respectively. It should be noticed that the independence of A and B is ensured by an independent sampling of the vectors of input factors. $V(Y)$ is computed using the outputs Y evaluated for both input matrices A and B.

S_{T_i} can be obtained simultaneously with S_i according to the method proposed by Jansen [20] and Saltelli et al.[14]:

$$S_{T_i} = \frac{\frac{1}{2N}\sum_{j=1}^{N} \left(f(A)_j - f\left(A_B^{(i)}\right)_j \right)^2}{V(Y)} \quad (9)$$

An in-house MATLAB-based program was developed to compute S_i and S_{T_i} according to Eqs. (8) and (9), respectively. Various values of the number of model executions N were used to evaluate and ensure the convergence of the computed SA indices.

2.C. TIAC input factors used in the sensitivity analysis

Activity data of a novel radiopharmaceutical ^{18}F-FSPG designed for positron emission tomography (PET) imaging of malignant diseases were employed in this work. The activity data were initially acquired by Smolarz et al.[23] from five healthy volunteers (two men, three women) and used for the development of the compartmental pharmacokinetic models for this agent, as reported elsewhere.[24] The 11 source regions for ^{18}F-FSPG included kidneys, bladder content, heart, thyroid, salivary glands, pancreas, stomach wall, liver, spleen, rest of body and blood.

The values of TIACs employed here were originally computed as the area under the organ time-activity curves predicted by compartmental pharmacokinetic models elsewhere[24] for the case of blood being a distinct source region. For ^{18}F-FSPG 11 TIAC input factors were considered, that is equal to the number of the source regions. Thus k = 11 in Eq. (3).

2.D. Employed anatomical models and SAF input factors

In this work, six human computational phantoms were considered. Table I summarizes the employed anatomical models, used abbreviations and the references to the original works describing them in detail. Figure 1 shows the anatomical models from Table I along with their body mass index (BMI).

TABLE I. Anatomical models of reference, slim, and overweight individuals employed for the SA study.

Description	Abbreviation	Reference
Voxel ICRP adult male reference computational phantom	RCP-AM	25
Polygon-surface ICRP adult male reference computational phantom	P-RCP-AM	26
Irene	Irene	27,28
Polygon-surface adult male computational phantom of a small individual	P-SCP-AM[a]	18
Visible Human	VisHuman	28
Polygon-surface adult male computational phantom of a big individual	P-BCP-AM[a]	18

[a]Note that P-SCP-AM and P-BCP-AM are denoted as Pat2M and Pat1M, respectively, in the referenced study.[18]

We used the SAFs of monoenergetic photon and electron sources calculated for the considered phantoms (see Table I and Fig. 1) with the Monte Carlo code EGSnrc[29] in our previous work.[18] Since the cross-sections for electrons and positrons of the same energies are very similar in the considered energy range of the β^+-spectrum of ^{18}F (from zero to the endpoint energy E_0 = 633.5 keV),[30] the SAFs of electron sources with the additional two 511 keV annihilation photons were used instead of the respective SAFs of positrons for the internal dosimetry in this work. The SAFs of monoenergetic electrons of various energies ranging from zero to E_0 were subsequently integrated over the detailed β^+-spectrum of ^{18}F from ICRP[16] to obtain the S-values according to Eq. (2). Thus, the SAFs of the discrete electron energies explicitly employed in the Monte Carlo calculations[18] were not considered as input factors in the SA. The S-values were used instead. Despite this simplification, for the sake of convenience these input factors are denoted SAF input factors, analogously to the photon component. For each radiation type, the number of considered sets of SAFs is equal to the number of source regions for the employed radiopharmaceutical. Thus, it is equal to 11 in case of ^{18}F-FSPG (see Section 2.C).

In the computational phantoms Irene and VisHuman, the heart wall was not segmented, and only the whole heart was available. Thus, heart wall was replaced by heart for these two phantoms. Breast of RCP-AM was employed for VisHuman, where no breast was present. Otherwise, as mentioned in Section 2.A, organs and tissues were excluded from the computation of weighted dose coefficients, when these regions were absent in at least one of the considered phantoms. For the urinary bladder dosimetry, the SAFs for photon and discrete electron energies computed by Andersson et al.[31] for the bladder content as source and bladder wall as target were employed here for all phantoms. Hence, no

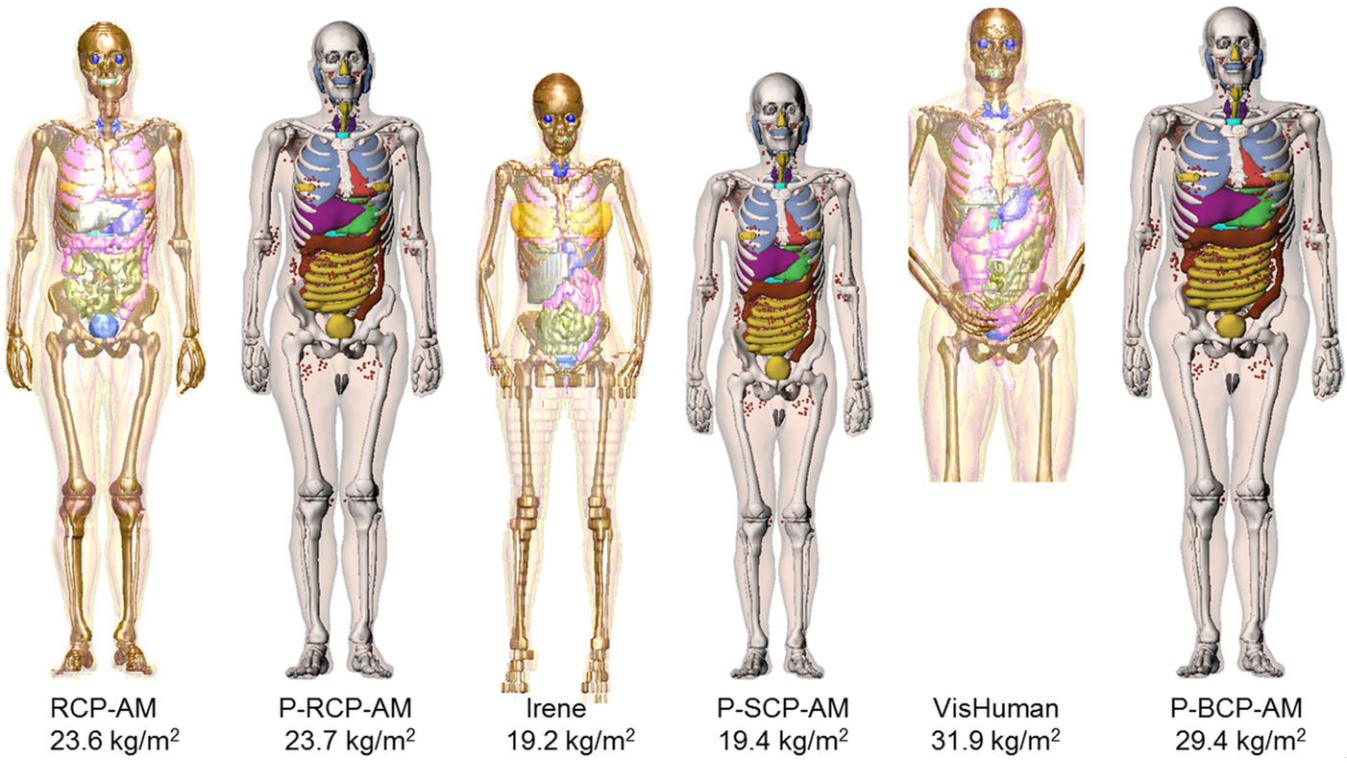

FIG. 1. Anatomical models of reference (RCP-AM and P-RCP-AM), slim (Irene and P-SCP-AM), and overweight (VisHuman and P-BCP-AM) individuals along with their BMI employed for the SA study.

variability of $SAF(UB_{wall} \leftarrow UB_{cont})$ among the anatomical models was considered (where UB_{wall} and UB_{cont} refer to urinary bladder wall and urinary bladder content, respectively). The mass-scaling of the SAFs to the reference organ masses of RCP-AM was applied.[17,18]

2.E. Sampling of the input factors

The low-discrepancy (also called quasi-random) sequence developed by Sobol'[32] was used to generate the samples of the independent variable input factors. Such deterministic sequences attempt to minimize the discrepancy, i.e., make the quasi-random points as well spaced as possible in a unit hypercube. Averaged over all projections in a multidimensional unit hypercube, the points in the Sobol' sequence[32] are distributed with a greater uniformity than random (or pseudo-random) numbers and, therefore, provide an accelerated convergence of the computed SA indices.

As described in Sections 2.C and 2.D, the considered model originally included 33 variable input factors for each model output: 11 TIAC and 22 SAF input factors (11 for photon- and 11 for β-components). For the same source–target pair, photon and electron SAFs cannot be considered uncorrelated inputs because they both depend on the positions of the source and the target relative to each other. For this reason the same quasi-random numbers were used for sampling the photon and the electron SAFs for the same combination of source and target regions. This decreased the dimensionality of the model from 33 to 22 dimensions.

A truncated normal distribution (without the negative tail) was assigned to the input factors. The parameters μ and σ (mean and standard deviation, respectively) of the probability density functions were computed from the five volunteer-specific sets of the TIACs for the TIAC input factors and from the phantom-specific sets of the SAFs for the SAF input factors. They are shown in Table II for the TIAC input factors. For the distributions of the SAF input factors for photons and electrons, the calculated parameters μ and σ are given in Tables III and IV, respectively.

We set the number of model runs to $N = 4096$. Thus, $N = 4096$ Sobol' quasi-random points[32] were generated for each of the independent matrices A and B in a 22-dimensional unit hypercube with a MATLAB-based program[33] distributed by the Joint Research Centre of the European Commission. The independent matrices A and B, each with a size of 4096×22, were generated according to the procedure described by Saltelli et al.[14] It was verified whether with this sample size the convergence of the computed sensitivity indices S_i and S_{T_i} was achieved, meaning whether S_i and S_{T_i} were numerically stable and their values changed only insignificantly with further increasing the number of model runs. Note that the size of a sample generated with deterministic quasi-random sequences in general and with the Sobol' sequence in particular can be increased if the convergence is not achieved with the originally selected number of model executions. The first N quasi-random (Sobol') numbers (and model executions) in the increased sample remain the same and, thus, they do not require model re-evaluation. The uniformly distributed Sobol' points were converted to the points from the desired truncated normal distributions with the precalculated parameters μ and σ using the inverse cumulative density function.

TABLE II. Mean μ [s] and standard deviation σ [s] of TIAC input factors distributions.

	Kidneys	Liver	Pancreas	Spleen	St-wall	Thyroid	S-glands	UB-cont	Ht-wall	RoB	Blood
μ	583.6	245.5	134.3	18.5	35.1	4.4	6.1	1175.4	44.3	1885.5	721.7
σ	79.2	88.2	33.6	9.7	15.2	1.1	1.2	123.2	25.2	392.8	118.5

St-wall stands for stomach wall; S-glands - for salivary glands; UB-cont - for urinary bladder content; Ht-wall - for heart wall; RoB - for rest of body.

3. RESULTS

Figure 2 shows mean values, standard deviations, and relative uncertainties in the computed absorbed dose coefficients and weighted dose coefficients. These uncertainties were caused by interindividual variability in TIACs and interphantom variability in SAFs (as shown in Tables II–IV).

Each sample in Fig. 2 includes $2N$=8192 dose coefficients calculated with both sampled matrices of input factors A and B (see Section 2.B). The relative uncertainty in weighted dose coefficient amounted to approximately 10%. The computed relative uncertainties in the absorbed dose coefficients were between 10% for urinary bladder wall and 30% for heart wall. Since one standard deviation was used to compute the relative uncertainties, for normally distributed values the presented error bars include approximately 68% of the $2N$ = 8192 dose coefficients.

Figure 3 shows the computed SA indices for the absorbed dose coefficient for spleen depending on the number of model executions. As it can be seen, with a small number of model runs, the SA indices were not stable and large fluctuations occurred. Nonetheless, both first-order and total-effect indices converged relatively fast. About 800 model runs were sufficient to achieve the convergence in this case. For other outputs the used number of model executions N = 4096 was also sufficient to ensure the convergence of the presented values S_i and S_{T_i}. Due to the relative simplicity of the model and the used implementation, the pure execution time of SA for the studied model with N = 4096 runs on a 3.10 GHz computer was approximately 0.05 s.

Figure 3 demonstrates that for spleen, which is a source region for ^{18}F-FSPG, TIAC(spleen) is the most influential parameter for the uncertainty in absorbed dose coefficient for spleen with S_i[TIAC(spleen)] = S_{T_i}[TIAC(spleen)] = 0.67. The influence of SAF(spleen ← blood) is also shown in Fig. 3 (S_i[SAF(spleen ← blood)] = 0.17 and S_{T_i}[SAF(spleen ← blood)] = 0.18). This result is consistent with the fact that spleen is a highly vascularized organ. It can be seen from Fig. 3 that no higher order effects were observed in this case, since the computed total-effect SA indices were approximately equal to the respective first-order effect indices.

A subset of the scatter plots and the respective SA indices for the absorbed dose coefficients for small intestine wall and lungs are presented in Figs. 4 and 5, respectively. Each point on a scatter plot represents an output calculated with one sampled vector of input factors ($TIAC_1$,$TIAC_2$,. . ., $TIAC_{11}$, SAF_1,SAF_2,. . .,SAF_{11}). Thus, each subplot of Figs. 4 and 5 contains N = 4096 points. The more prominent patterns in the scatter plots correspond to the more influential input factors, making such plots a convenient graphical representation of the sensitivity.

Being target regions and not sources for ^{18}F-FSPG, small intestine wall and lungs receive radiation doses from the cross-fire from other source regions. The example in Fig. 4 shows that the uncertainty in the output was mainly caused by the variability in the cross-fire SAFs from the proximal sources, for example, SAF(small intestine wall ← UB_{cont}) for absorbed dose coefficient for small intestine wall, where S_i[SAF(small intestine wall ← UB_{cont})] = 0.75 and S_{T_i} for the same input factor was 0.76. For lungs, as for a target region with substantial mass fraction of blood, notable effect of SAF (r_T ← blood) and TIAC(blood) was found and quantitatively expressed via the computed S_i and S_{T_i} values shown in Fig. 5: S_i[SAF(lungs ← blood)] = 0.71, S_{T_i}[SAF(lungs ← blood)] = 0.73, S_i[TIAC(blood)] = 0.19 and S_{T_i}[TIAC(blood)] = 0.21.

Figure 6 shows the first-order effect SA indices for all considered target regions. Each horizontal line in Fig. 6 contains S_i in gray color-codes for all input factors and a selected output. Figure 6 breaks down the uncertainty in each output dose coefficient presented in Fig. 2 into parts caused by each input factor variability. In Fig. 6, these contributions are numerically expressed by the corresponding values of S_i. The computed total-effect SA indices were similar to those of the first-order and, thus, are not presented here. The similarity of main and total-effect SA indices indicates that no substantial higher order effects were observed in the model. Another indication of the absence of notable higher order effects in the studied model is that $\sum_{i=1}^{2k} S_i \approx 1$.

Several trends can be seen from Fig. 6. The uncertainty in the computed doses for the source regions was dominated or, in some cases, solely defined by the variability in the activities accumulated in the respective source regions (see the diagonal line of high S_i in the lower left corner of Fig. 6). The results showed that for the target regions, which are not sources, the most influential factors for the uncertainty in the computed doses were the cross-fire SAFs from proximal sources. For example, the variability in SAF(adrenals ← kidneys) had the greatest impact on the uncertainty in the absorbed dose coefficient for adrenals (S_i[SAF(adrenals ← kidneys)] = 0.60) and the variability in SAF(r_T ← UB_{cont}) on the absorbed dose coefficients for small intestine wall (S_i[SAF(small intestine wall ← UB_{cont})] = 0.60), gonads (S_i[SAF(gonads ← UB_{cont})] = 0.59) and colon wall (S_i[SAF (colon wall ← UB_{cont})] = 0.27). To a lesser extent, but nonetheless non-negligible, was the influence of the integrated activities accumulated in the proximal source regions, for example for adrenals and gonads, S_i[TIAC

TABLE III. Mean μ [g^{-1}] and standard deviation σ [g^{-1}] of SAF input factors distributions for photons.

	Source regions										
Target regions	Kidneys	Liver	Pancreas	Spleen	St-wall	Thyroid	S-glands	UB-cont	Ht-wall	RoB	Blood
Kidneys											
μ	2.5E-04	2.2E-05	3.6E-05	3.2E-05	1.7E-05	9.3E-07	3.3E-07	1.6E-06	5.6E-06	4.0E-06	1.6E-05
σ	3.8E-06	6.4E-06	1.5E-05	9.9E-06	6.7E-06	1.0E-07	3.5E-08	1.8E-07	1.2E-06	8.5E-07	4.0E-06
Liver											
μ	2.2E-05	9.2E-05	3.4E-05	6.7E-06	2.1E-05	2.3E-06	7.4E-07	7.5E-07	1.6E-05	2.5E-06	2.0E-05
σ	6.4E-06	9.2E-07	7.2E-06	1.7E-06	4.6E-06	3.1E-07	7.0E-08	1.9E-07	2.7E-06	9.8E-07	4.5E-06
Pancreas											
μ	3.6E-05	3.4E-05	4.9E-04	2.0E-05	6.7E-05	1.2E-06	4.2E-07	1.3E-06	1.2E-05	3.8E-06	1.7E-05
σ	1.5E-05	7.2E-06	2.3E-05	1.3E-05	3.1E-05	1.3E-07	6.1E-08	3.3E-07	2.4E-06	7.6E-07	4.5E-06
Spleen											
μ	3.2E-05	6.7E-06	2.0E-05	4.8E-04	4.3E-05	2.4E-06	7.7E-07	5.3E-07	1.5E-05	3.4E-06	1.7E-05
σ	9.9E-06	1.7E-06	1.3E-05	1.3E-05	1.4E-05	3.5E-07	7.1E-08	7.3E-08	4.7E-06	7.7E-07	4.2E-06
St-wall											
μ	1.7E-05	2.1E-05	6.7E-05	4.3E-05	2.6E-04	2.0E-06	6.6E-07	7.5E-07	2.9E-05	3.4E-06	1.5E-05
σ	6.7E-06	4.6E-06	3.1E-05	1.4E-05	3.2E-05	2.5E-07	1.1E-07	1.7E-07	4.8E-06	7.5E-07	3.4E-06
Thyroid											
μ	9.0E-07	2.3E-06	1.2E-06	2.3E-06	1.9E-06	1.5E-03	1.7E-05	4.7E-08	9.9E-06	4.3E-06	7.5E-06
σ	1.1E-07	3.2E-07	1.3E-07	3.6E-07	2.3E-07	3.6E-05	2.5E-06	8.5E-09	1.1E-06	8.1E-07	1.7E-06
S-glands											
μ	3.1E-07	7.1E-07	3.8E-07	7.3E-07	6.2E-07	1.7E-05	4.6E-04	1.8E-08	1.8E-06	3.8E-06	4.0E-06
σ	4.5E-08	6.7E-08	5.9E-08	7.1E-08	1.1E-07	2.5E-06	2.1E-05	2.8E-09	1.5E-07	9.9E-07	9.8E-07
UB-wall											
μ	1.5E-06	7.3E-07	1.2E-06	5.1E-07	7.1E-07	4.3E-08	2.0E-08	2.5E-04	2.3E-07	5.4E-06	4.8E-06
σ	1.7E-07	2.0E-07	2.7E-07	7.5E-08	1.5E-07	6.1E-09	3.4E-09	0.0E+00	3.7E-08	6.4E-07	1.7E-06
Ht-wall											
μ	5.6E-06	1.6E-05	1.2E-05	1.5E-05	2.9E-05	1.0E-05	1.8E-06	2.4E-07	1.6E-04	3.5E-06	2.2E-05
σ	1.2E-06	2.7E-06	2.4E-06	4.8E-06	4.8E-06	1.1E-06	1.4E-07	4.7E-08	2.5E-06	8.4E-07	5.8E-06
Red marrow											
μ	8.1E-06	6.6E-06	8.3E-06	7.5E-06	5.7E-06	9.6E-06	5.9E-06	9.1E-06	8.0E-06	5.6E-06	7.2E-06
σ	1.6E-06	1.2E-06	2.2E-06	1.2E-06	1.3E-06	2.2E-06	1.6E-06	1.3E-06	1.6E-06	9.1E-07	1.8E-06
Colon											
μ	1.5E-05	1.0E-05	2.1E-05	9.3E-06	1.8E-05	4.9E-07	1.9E-07	1.6E-05	3.2E-06	5.0E-06	9.7E-06
σ	3.2E-06	2.0E-06	6.0E-06	1.7E-06	4.3E-06	1.0E-07	3.4E-08	4.1E-06	6.0E-07	9.4E-07	1.9E-06
Lungs											
μ	4.7E-06	1.3E-05	6.8E-06	1.6E-05	1.2E-05	1.5E-05	2.8E-06	1.9E-07	3.3E-05	4.2E-06	1.6E-05
σ	8.3E-07	2.0E-06	1.7E-06	3.5E-06	2.0E-06	2.5E-06	3.9E-07	3.4E-08	6.1E-06	7.0E-07	3.5E-06
Esophagus											
μ	5.3E-06	1.3E-05	9.9E-06	1.2E-05	1.8E-05	1.0E-04	7.3E-06	1.8E-07	6.1E-05	4.8E-06	1.7E-05
σ	7.0E-07	3.1E-06	1.6E-06	2.3E-06	3.1E-06	2.6E-05	1.3E-06	4.0E-08	1.3E-05	8.7E-07	3.4E-06
Brain											
μ	9.9E-08	2.3E-07	1.1E-07	2.4E-07	1.8E-07	2.8E-06	1.6E-05	5.6E-09	4.8E-07	4.6E-06	2.9E-06
σ	1.3E-08	1.4E-08	1.8E-08	2.2E-08	3.2E-08	2.3E-07	2.3E-06	1.1E-09	4.5E-08	1.1E-06	7.9E-07
Adrenals											
μ	1.1E-04	3.4E-05	7.7E-05	5.6E-05	3.0E-05	1.5E-06	5.1E-07	8.9E-07	1.1E-05	4.4E-06	1.6E-05
σ	2.8E-05	6.1E-06	6.9E-05	1.7E-05	1.7E-05	1.6E-07	4.1E-08	1.0E-07	2.5E-06	6.9E-07	4.3E-06
Small intestine											
μ	1.4E-05	6.0E-06	2.3E-05	6.0E-06	1.1E-05	3.4E-07	1.3E-07	2.1E-05	2.5E-06	5.5E-06	9.9E-06
σ	4.2E-06	8.7E-07	1.0E-05	2.2E-06	3.8E-06	1.2E-07	4.5E-08	1.4E-05	8.6E-07	1.1E-06	1.8E-06

St-wall denotes stomach wall; S-glands - salivary glands; UB-wall - urinary bladder wall; Ht-wall - heart wall; UB-cont - urinary bladder content; RoB - rest of body.

TABLE IV. Mean μ [MeV·g^{-1}][a] and standard deviation σ [MeV·g^{-1}][a] of SAF input factors distributions for electrons.

	Source regions										
Target regions	Kidneys	Liver	Pancreas	Spleen	St-wall	Thyroid	S-glands	UB-cont	Ht-wall	RoB	Blood
Kidneys											
μ	7.6E-04	6.1E-08	1.4E-07	1.2E-07	5.3E-09	1.2E-10	2.6E-11	2.0E-10	1.2E-09	0.0E+00	2.1E-05
σ	1.8E-06	5.6E-08	2.8E-07	2.4E-07	2.5E-09	1.8E-11	4.9E-12	4.1E-11	3.0E-10	0.0E+00	7.7E-06
Liver											
μ	6.1E-08	1.3E-04	7.3E-08	1.5E-09	1.8E-07	4.0E-10	8.7E-11	7.7E-11	1.5E-08	0.0E+00	1.9E-05
σ	5.6E-08	5.2E-07	7.7E-08	4.8E-10	8.1E-08	6.4E-11	1.1E-11	2.4E-11	1.4E-08	0.0E+00	6.6E-06
Pancreas											
μ	1.4E-07	7.3E-08	1.7E-03	6.0E-08	1.7E-06	1.7E-10	4.1E-11	1.7E-10	3.2E-09	2.1E-07	1.3E-05
σ	2.8E-07	7.7E-08	9.1E-06	1.2E-07	2.2E-06	2.8E-11	1.5E-11	7.0E-11	7.7E-10	3.1E-07	3.9E-06
Spleen											
μ	1.2E-07	1.5E-09	5.9E-08	1.6E-03	2.7E-07	4.2E-10	8.1E-11	4.2E-11	4.7E-09	0.0E+00	2.6E-05
σ	2.4E-07	4.9E-10	1.2E-07	7.0E-06	5.1E-07	7.0E-11	1.2E-11	1.1E-11	1.8E-09	0.0E+00	9.0E-06
St-wall											
μ	5.3E-09	1.8E-07	1.7E-06	2.7E-07	1.5E-03	3.3E-10	7.2E-11	7.6E-11	4.8E-07	0.0E+00	1.5E-05
σ	2.5E-09	8.1E-08	2.2E-06	5.2E-07	2.1E-05	6.1E-11	2.1E-11	2.0E-11	3.7E-07	0.0E+00	4.5E-06
Thyroid											
μ	8.3E-11	4.2E-10	1.7E-10	4.4E-10	3.1E-10	1.2E-02	4.3E-09	3.0E-12	2.5E-09	0.0E+00	8.7E-06
σ	1.5E-11	9.5E-11	3.5E-11	6.9E-11	6.4E-11	4.8E-05	6.3E-10	4.4E-12	3.9E-10	0.0E+00	2.8E-06
S-glands											
μ	2.5E-11	8.5E-11	2.9E-11	8.8E-11	6.3E-11	4.1E-09	2.7E-03	1.6E-13	2.8E-10	4.4E-07	1.0E-05
σ	8.9E-12	1.4E-11	5.5E-12	3.0E-11	1.5E-11	7.9E-10	1.4E-05	2.6E-13	4.8E-11	5.2E-07	3.3E-06
UB-wall											
μ	1.8E-10	6.6E-11	1.4E-10	4.4E-11	6.8E-11	2.4E-12	7.6E-13	4.8E-05	1.4E-11	3.2E-06	1.3E-06
σ	5.3E-11	2.2E-11	4.5E-11	1.4E-11	2.2E-11	2.2E-12	1.1E-12	0.0E+00	8.0E-12	3.6E-07	4.3E-07
Ht-wall											
μ	1.2E-09	1.5E-08	3.1E-09	4.7E-09	4.8E-07	2.5E-09	2.9E-10	1.5E-11	5.6E-04	4.6E-08	6.1E-06
σ	3.1E-10	1.4E-08	7.2E-10	1.9E-09	3.7E-07	3.2E-10	2.8E-11	4.1E-12	1.9E-04	6.5E-08	5.2E-06
Red marrow											
μ	6.4E-09	1.3E-08	1.0E-08	8.6E-09	2.4E-09	3.6E-08	2.4E-08	2.0E-08	6.4E-09	3.4E-06	3.5E-06
σ	7.1E-09	1.4E-08	1.7E-08	8.2E-09	1.0E-09	7.4E-08	4.2E-08	3.4E-08	2.4E-09	3.6E-07	2.7E-06
Colon											
μ	6.8E-08	4.7E-08	1.8E-08	4.8E-08	1.1E-07	5.4E-11	1.5E-11	1.1E-08	6.7E-10	2.4E-06	1.6E-05
σ	1.2E-07	4.5E-08	2.2E-08	8.8E-08	1.4E-07	1.7E-11	4.5E-12	1.1E-08	1.8E-10	3.3E-07	5.3E-06
Lungs											
μ	1.0E-09	1.5E-07	1.6E-09	1.9E-07	8.8E-08	4.7E-09	4.6E-10	1.2E-11	4.4E-07	1.6E-06	3.1E-05
σ	2.1E-10	1.0E-07	5.1E-10	1.5E-07	1.2E-07	9.5E-10	7.5E-11	2.5E-12	2.7E-07	5.5E-07	1.2E-05
Esophagus											
μ	1.2E-09	3.7E-08	2.9E-09	3.5E-09	1.9E-07	2.5E-06	1.7E-09	1.4E-11	1.4E-06	2.6E-06	1.5E-05
σ	2.1E-10	3.8E-08	6.7E-10	8.5E-10	3.8E-07	3.0E-06	4.0E-10	3.3E-12	1.4E-06	3.2E-07	4.6E-06
Brain											
μ	4.6E-12	1.5E-11	5.6E-12	1.4E-11	1.1E-11	3.3E-10	3.0E-09	1.6E-13	4.0E-11	3.4E-06	2.7E-06
σ	6.4E-13	1.4E-12	1.1E-12	1.2E-12	2.0E-12	2.5E-11	5.3E-10	1.3E-13	4.8E-12	4.1E-07	7.2E-07
Adrenals											
μ	7.3E-06	4.4E-07	3.2E-06	7.8E-08	1.1E-08	2.0E-10	3.6E-11	7.2E-11	2.8E-09	2.7E-06	1.3E-05
σ	5.1E-06	4.3E-07	5.2E-06	1.2E-07	7.0E-09	3.9E-11	1.3E-11	1.9E-11	7.2E-10	3.3E-07	3.9E-06
Small intestine											
μ	2.8E-08	3.4E-09	4.5E-07	6.8E-09	1.0E-07	3.6E-11	7.9E-12	8.2E-08	5.1E-10	2.4E-06	1.6E-05
σ	2.8E-08	4.4E-09	6.0E-07	1.2E-08	1.2E-07	1.6E-11	4.0E-12	1.3E-07	2.2E-10	3.2E-07	5.1E-06

St-wall denotes stomach wall; S-glands - salivary glands; UB-wall - urinary bladder wall; Ht-wall - heart wall; UB-cont - urinary bladder content; RoB - rest of body.
[a]SAF input factors for β-component denote, for simplicity, the corresponding *S*-values integrated over the β^+-spectrum. Thus, these values are in units [MeV·g^{-1}] in contrast to the SAF input factors for photon component. See Section 2.D for more details.

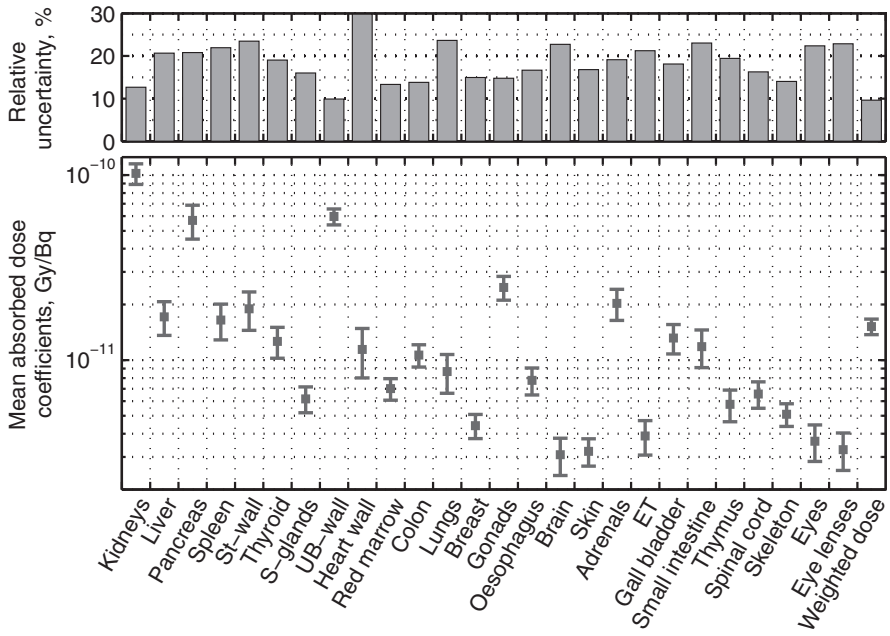

FIG. 2. Computed dose coefficients along with their uncertainties. Each error bar on the lower panel represents one standard deviation of the respective dose coefficient. The SAFs are mass-scaled to the reference masses of RCP-AM. St-wall denotes stomach wall; S-glands - salivary glands; UB-wall - urinary bladder wall; ET - extrathoracic airways.

(kidneys)] = 0.14 and S_i[TIAC(UB_{cont})] = 0.32, respectively. For the targets that do not have high blood contents and are located distantly from the source regions, e.g., eyes, eye lenses, skeleton, skin, extrathoracic airways (ET), or brain, the variability of TIAC(r_{RoB}) was an important factor, contributing to the uncertainty in the absorbed dose coefficients (see Fig. 6). For the organs with substantial mass fractions of blood, the SA indices for the input factors SAF($r_T \leftarrow$ blood) and TIAC(blood) amounted to high values (see Figs. 5 and 6). This illustrates the importance of an accurate determination of SAF($r_T \leftarrow$ blood) and blood activities in dosimetric studies in nuclear medicine. The change in SAF($r_T \leftarrow$ blood) had the highest impact on the uncertainty in the weighted dose coefficient (Fig. 6) with $S_i = S_{T_i} = 0.31$. Each of the variable input factors TIAC($St - wall$), TIAC(UB_{cont}), TIAC (blood), TIAC(r_{RoB}), and SAF($r_T \leftarrow UB_{cont}$) accounted for approximately 10% of the variance of the weighted dose coefficient.

4. DISCUSSION

The global variance-based SA allows studying the interplay effects of any possible simultaneous perturbation of the inputs on the variance of the model output. It does not require the studied model to be analytical. All these aspects make the global variance-based SA superior compared to more frequently used OAT or Gaussian error propagation.

As part of the Monte Carlo-based SA approach implemented in this work, the uncertainties in the absorbed dose coefficients for various target regions were computed. Two sources of uncertainties were investigated: the interindividual variability in the TIACs and the differences among the anatomical models employed for dosimetry. The TIACs were computed based on the individual-specific pharmacokinetic models in our previous work.[24] The pharmacokinetic models were assumed to be fixed. Thus, the uncertainties associated with the model structure were neglected. Another limitation of this work is the omission of several sources of uncertainties related to image acquisition and image quantification that might be more important, in particular for SPECT systems. Therefore, the overall uncertainties in the organ absorbed doses are potentially larger than the reported values. The variability in the tissue weighting factors[19] employed in the computation of weighted dose coefficients was not considered. Xie and Zaidi[34] investigated another source of uncertainty in the computed organ doses associated with respiratory motion. Despite this effect being negligible for most organs considered by Xie and Zaidi,[34] the authors reported cases where it can be perceptible. Although consideration of all of the foregoing sources of uncertainties is of interest, it is beyond the scope of the current study.

Six anatomical models representing slim, reference and overweight individuals were employed in this study to construct the distributions of the SAF input factors. The models covered the range in the BMI from 19.2 to 31.9 kg/m^2. Although it cannot be claimed that all possible anatomic variations were covered, the considered interphantom differences were not limited to the six employed models. The tails of the normal distributions assigned to the input factors covered a broader range of SAFs than that of the six considered phantoms. The Sobol' sequence ensured the sampling of the input factors also from the less probable areas of the input space. The same holds true for the variations of the TIAC input factors, whose distributions were constructed based on the

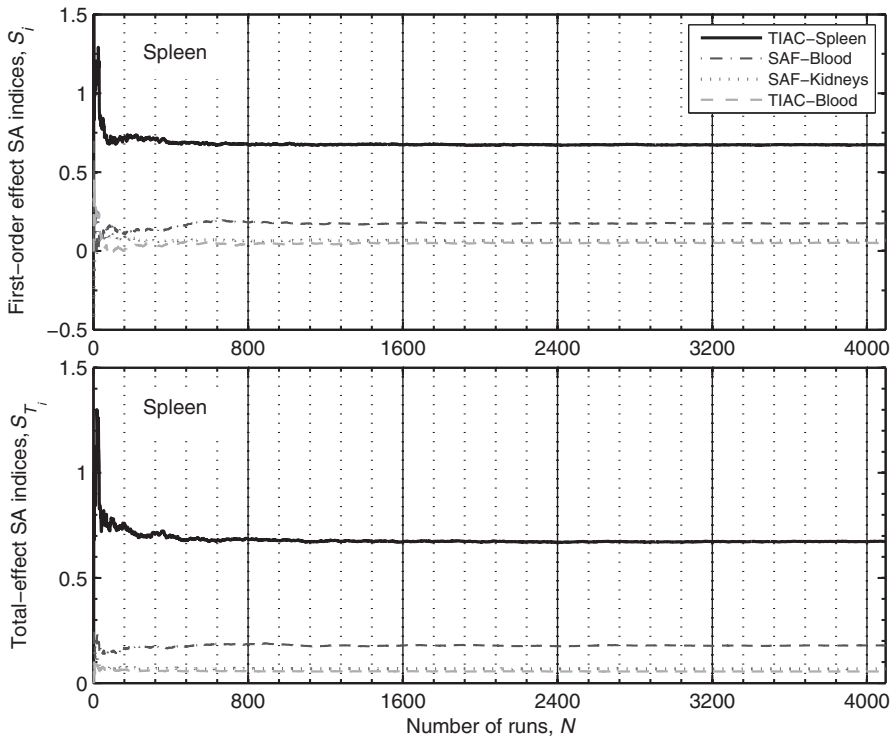

FIG. 3. Convergence plots for the first-order (top) and the total-effect (bottom) SA indices for absorbed dose coefficient for spleen. From the overall 22 convergence curves (11 TIAC and 11 SAF input factors), only those four for the input factors with first-order and total-effect SA indices above 0.05 are displayed (see legend). Note that $SAF(spleen \leftarrow spleen)$ of all phantoms were corrected to correspond to the mass of spleen in RCP-AM.

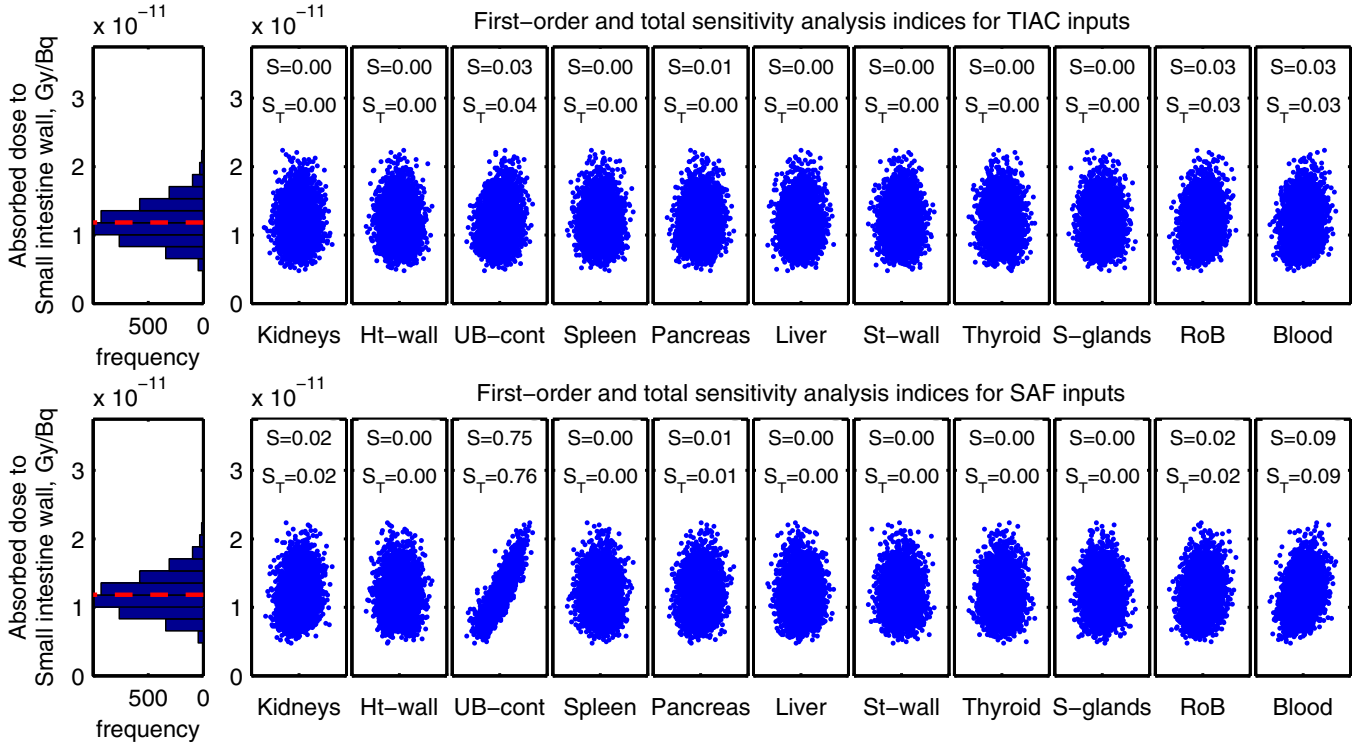

FIG. 4. Scatter plots, SA indices, and distribution of absorbed dose coefficient for small intestine wall. Upper row corresponds to the TIAC input factors, lower row to the SAF input factors. The values S and S_T are the first-order and the total SA indices, respectively. The histogram displays the distribution of the output dose coefficient. The mean value of the computed absorbed dose coefficient for small intestine wall is marked with red dashed line (online version only).

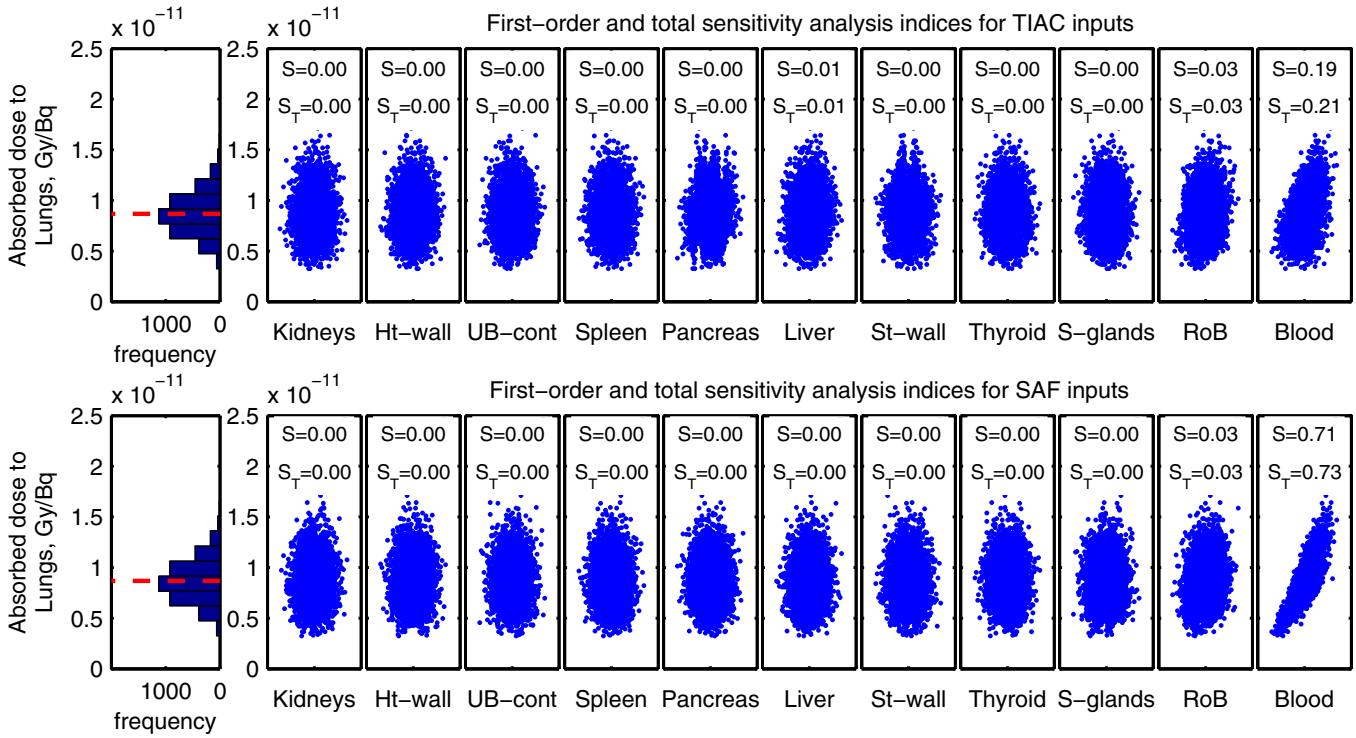

FIG. 5. Analogue to Fig. 4, scatter plots, SA indices, and distribution of absorbed dose coefficient for lungs. The mean value of the computed absorbed dose coefficient for lungs is marked with red dashed line (online version only).

activity data of five volunteers. Thus, it is reasonable to assume that the considered differences in the input factors are an adequate estimate for their variability.

The uncertainty in the absorbed dose coefficient for bladder wall was the lowest, since the same values of SAF($UB_{wall} \leftarrow UB_{cont}$) calculated by Andersson et al.[31] were used for all phantoms. Thus, the uncertainty in the output in this case was caused predominantly by the variability of TIAC(UB_{cont}). The utilization of SAF($UB_{wall} \leftarrow UB_{cont}$) derived by Andersson et al.[31] was more appropriate here rather than the usage of the corresponding phantom-specific values. For a certain type of radiation and energy, the foregoing SAFs are dependent on the volumes of the bladder content and the thickness of the bladder wall. Thus, if the phantom-specific values of SAF($UB_{wall} \leftarrow UB_{cont}$) were used, the differences in the bladder volumes segmented in the phantoms and in the thickness of the bladder wall, which is often limited by the voxel size, would introduce additional artificial variation in the SAF input factors. Although a dynamic bladder model would be more appropriate for the estimation of doses to the bladder wall, the application of variance-based SA to this model is beyond the scope of the current work. The highest uncertainty was observed for heart wall absorbed dose coefficient. The reason for this was a high interindividual difference in TIAC(*Ht – wall*) and the fact that heart wall of two phantoms was modeled as the whole heart.

Computational phantoms with all required regions segmented and blood properly distributed in various body organs are to be used in the SA. Otherwise, additional artificial variations in the SAF input factors could be introduced and lead to different and possibly inadequate results of the SA. For this reason, no organ surrogates, besides the whole heart for the heart wall, were used in this work, and organs that are not present in one or more phantoms were omitted, except the breast of the VisHuman for which the SAF values of the RCP-AM have been used. The value denoted as weighted dose coefficient was an adequate estimate for the effective dose coefficient. Only few target regions were excluded (see Section 2.A). Since these regions are not notable sources for ^{18}F-FSPG, the expected absolute absorbed dose coefficients for them are not high. The corresponding tissue weighting factors are also relatively low (0.01 for endosteum and approximately 0.006 for other regions that are part of the remainder tissues).

The absorbed dose coefficient for each source region r_S was, of course, highly dependent on the TIAC(r_S). For the relatively low energies of the β^+-spectrum of ^{18}F the dose absorbed in r_S is mainly due to the self-absorption in this region. The applied mass-scaling of the self-absorption SAFs eliminated the interphantom variability in these values and thus the uncertainty in the output dose coefficients for r_S was mainly caused by the variability in the respective TIACs. Considering the sources of uncertainties related to activity quantification would increase the overall variability in TIACs, and hence the shown effect of TIACs would potentially become even more prominent. Thus the accurate determination of TIAC(r_S) substantially improves the accuracy of the computed absorbed dose coefficients for source regions r_S. It also implicitly includes the estimation of the source region masses needed for mass-scaling of the self-absorption SAFs. A high importance of SAF($r_T \leftarrow$ blood) for the organs with

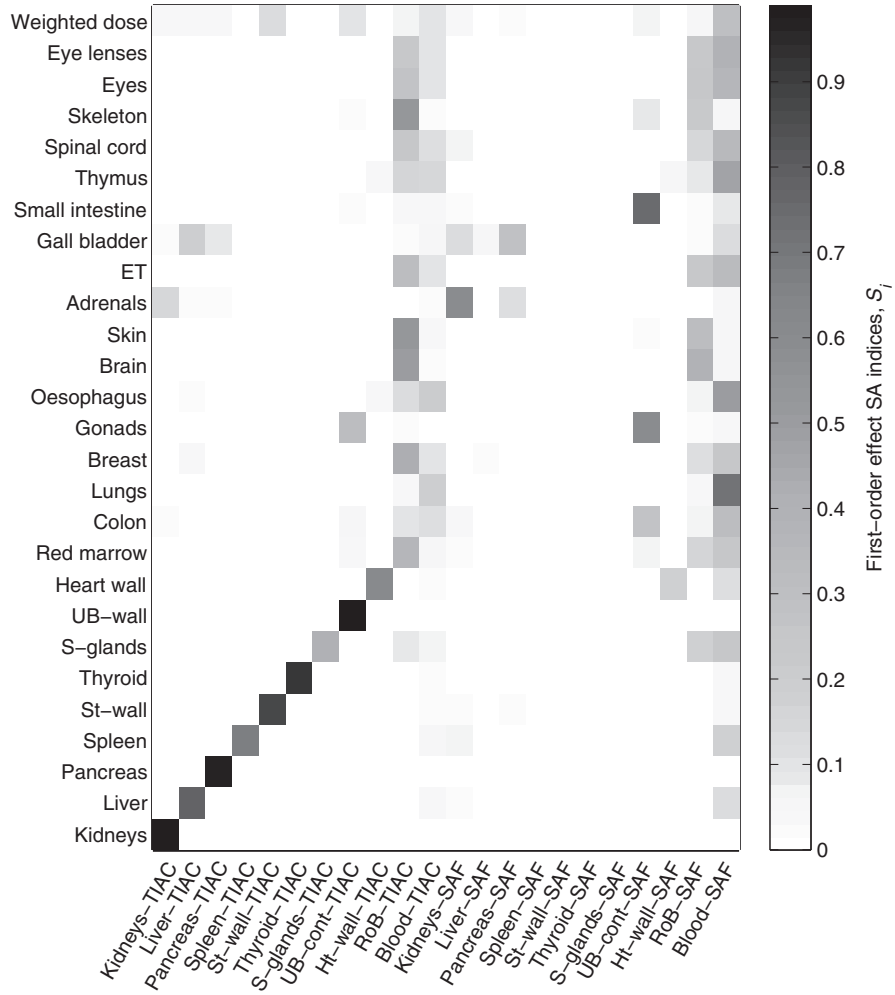

FIG. 6. First-order effect SA indices for all considered outputs. The input factors are plotted from left to right and the output target regions from bottom to top. $S_i = 0$ means no main effect of the corresponding input factor. $S_i = 1$ means that the uncertainty in the output is solely caused by the variability of the corresponding input factor.

substantial mass fraction of blood was observed. The values of SAF($r_T \leftarrow$ blood) are independent of the relative positions of organs in anatomical models though. They are defined by the blood contents of the respective organs r_T. This shows that the determination of the individual blood contents of organs has the potential to notably decrease the uncertainty in the computed absorbed doses for highly vascularized organs.

Although the MIRD schema includes the product of the input factors TIAC(r_S) and $SAF(r_T \leftarrow r_S)$, no considerable higher order effects were observed. This was due to very low absolute values of $SAF(r_T \leftarrow r_S)$ compared to TIAC(r_S) in case $r_T \neq r_S$ and negligible variability in $SAF(r_T \leftarrow r_S)$ when $r_T = r_S$.

In this work the available activity data of a radiopharmaceutical designated for PET diagnosis were employed. Although the agent used is rather exotic compared to such radiopharmaceuticals as ^{18}F-FDG, we believe that some of the results obtained for ^{18}F-FSPG hold true for other agents distributed via blood (e.g., a high importance of TIAC(r_S) for source regions r_S and SAF($r_T \leftarrow$ blood) for the organs with substantial mass fraction of blood). The example considered is a dosimetry study with a diagnostic agent. The overall level of accuracy required for dosimetry in a diagnostic study is lower than that for patients undergoing radiopharmaceutical therapy. Nonetheless, the developed framework is independent of the radiopharmaceutical used. The applied methods could be extended to therapeutic agents taking into account the differences in dosimetry approach (e.g., using patient-individual geometries instead of generic computational phantoms).

5. CONCLUSIONS

The global SA is a powerful model-independent method to investigate the effect on the model output of simultaneous changes of the variable input factors. It accounts for the possible interactions in the model and effectively explores the input space. Such variance-based SA, accompanied by an uncertainty analysis as part of its procedure, was applied in this work to internal dosimetry in nuclear medicine according to the MIRD schema. For each output organ absorbed dose coefficient an uncertainty along with the set of the first-order and total-effect SA indices were computed. The results of this investigation show that uncertainties in the estimated absorbed dose coefficients for source regions are dominated or, in some cases,

solely caused by the variability in the respective TIACs, if applying mass-scaling of the SAFs. Such mass-scaling requires the knowledge of total body mass and masses of individual source regions, which are typically determined as part of the procedure of absolute activity quantification. A high impact of SAFs for blood as a source region was shown for organs with substantial mass fractions of blood and for the computed weighted dose coefficient. The results indicate the potential to notably reduce uncertainties in computed absorbed doses in nuclear medicine by the usage of proper blood distribution in a patient's body, accurate determination of TIACs, and source region masses and — in a few cases — by the accurate estimation of the cross-fire SAFs from proximal source regions.

ACKNOWLEDGMENT

The work was supported by the German Bundesministerium für Bildung und Forschung, grant 02NUK026.

We thank Dr. Weibo Li for fruitful discussions on sensitivity analysis.

CONFLICTS OF INTEREST

The authors have no conflicts to disclose.

[a]Author to whom correspondence should be addressed. Electronic mail: azvereva@bfs.de, Telephone: +49(0)30 18 333-2343, Fax: +49(0)30 18 333-2305.

REFERENCES

1. Bolch WE, Eckerman KF, Sgouros G, Thomas SR. MIRD pamphlet No. 21: a generalized schema for radiopharmaceutical dosimetry–standardization of nomenclature. *J Nucl Med*. 2009;50:477–484.
2. Stabin MG. Update: the case for patient-specific dosimetry in radionuclide therapy. *Cancer Biother Radiopharm*. 2008;23:273–284.
3. Flux G, Bardies M, Chiesa C, et al. Clinical radionuclide therapy dosimetry: the quest for the "Holy Gray". *Eur J Nucl Med Mol Imaging*. 2007;34:1699–1700.
4. Mattsson S. Patient dosimetry in nuclear medicine. *Radiat Prot Dosimetry*. 2015;165:416–423.
5. Paquet F, Bailey MR, Leggett RW, Harrison JD. Assessment and interpretation of internal doses: uncertainty and variability. *Ann ICRP*. 2016;45(1 Suppl):202–214.
6. NCRP. Uncertainties in internal radiation dose assessment, NCRP Report No. 164; 2009.
7. Stabin MG. Uncertainties in internal dose calculations for radiopharmaceuticals. *J Nucl Med*. 2008;49:853–860.
8. Spielmann V, Li WB, Zankl M, Oeh U, Hoeschen C. Uncertainty quantification in internal dose calculations for seven selected radiopharmaceuticals. *J Nucl Med*. 2016;57:122–128.
9. Saltelli A, Annoni P. How to avoid a perfunctory sensitivity analysis. *Environ Modell Softw*. 2010;25:1508–1517.
10. Saltelli A, Ratto M, Andres T, et al. *Global Sensitivity Analysis: The Primer*. Hoboken, NJ: John Wiley & Sons; 2008.
11. Ferretti F, Saltelli A, Tarantola S. Trends in sensitivity analysis practice in the last decade. *Sci Total Environ*. 2016;568:666–670.
12. Sobol' IM. Sensitivity estimates for nonlinear mathematical models. *Matematicheskoe Modelirovanie*. 1990;2:112–118.
13. Sobol' IM. Global sensitivity indices for nonlinear mathematical models and their Monte Carlo estimates. *Math Comput Simulat*. 2001;55:271–280.
14. Saltelli A, Annoni P, Azzini I, Campolongo F, Ratto M, Tarantola S. Variance based sensitivity analysis of model output. Design and estimator for the total sensitivity index. *Comput Phys Commun*. 2010;181:259–270.
15. Li WB, Hoeschen C. Uncertainty and sensitivity analysis of biokinetic models for radiopharmaceuticals used in nuclear medicine. *Radiat Prot Dosimetry*. 2010;139:228–231.
16. ICRP. Nuclear decay data for dosimetric calculations, ICRP Publication 107; 2008.
17. Snyder WS, Ford MR, Warner GG, Watson EE. "S" absorbed dose per unit cumulated activity for selected radionuclides and organs, MIRD Pamphlet 1975.
18. Zvereva A, Schlattl H, Zankl M, et al. Feasibility of reducing differences in estimated doses in nuclear medicine between a patient-specific and a reference phantom. *Phys Med*. 2017;39:100–112.
19. ICRP. The 2007 Recommendations of the International Commission on Radiological Protection. ICRP Publication. 103:2007.
20. Jansen MJW. Analysis of variance designs for model output. *Comput Phys Commun*. 1999;117:35–43.
21. Homma T, Saltelli A. Importance measures in global sensitivity analysis of nonlinear models. *Reliab Eng Syst Safe*. 1996;52:1–17.
22. Saltelli A, Tarantola S. On the relative importance of input factors in mathematical models: Safety assessment for nuclear waste disposal. *J Am Stat Assoc*. 2002;97:702–709.
23. Smolarz K, Krause BJ, Graner FP, et al. (S)-4-(3-18F-fluoropropyl)-L-glutamic acid: an 18F-labeled tumor-specific probe for PET/CT imaging–dosimetry. *J Nucl Med*. 2013;54:861–866.
24. Zvereva A, Petoussi-Henss N, Li WB, et al. Effect of blood activity on dosimetric calculations for radiopharmaceuticals. *Phys Med Biol*. 2016;61:7688–7703.
25. ICRP. Adult reference computational phantoms, ICRP Publication 110; 2009.
26. Yeom YS, Han MC, Kim CH, Jeong JH. Conversion of ICRP male reference phantom to polygon-surface phantom. *Phys Med Biol*. 2013;58:6985–7007.
27. Fill U, Zankl M, Petoussi-Henss N, Siebert M, Regulla D. Adult female voxel models of different stature and photon conversion coefficients for radiation protection. *Health Phys*. 2004;86:253–272.
28. Zankl M, Fill U, Petoussi-Henss N, Regulla D. Organ dose conversion coefficients for external photon irradiation of male and female voxel models. *Phys Med Biol*. 2002;47:2367–2385.
29. Kawrakow I, Rogers DWO. The EGSnrc code system: Monte Carlo simulation of electron and photon transport, 2003.
30. ICRU. Stopping powers for electrons and positrons, ICRU Report; 1984.
31. Andersson M, Minarik D, Johansson L, Mattsson S, Leide-Svegborn S. Improved estimates of the radiation absorbed dose to the urinary bladder wall. *Phys Med Biol*. 2014;59:2173–2182.
32. Sobol' IM. On the distribution of points in a cube and the approximate evaluation of integrals. *USSR Comput Math & Math Phys*. 1967;7:86–112.
33. Sobol' IM, Turchaninov VI, Levitan YL, Shukhman BV. Quasi-random sequence generators, 1992.
34. Xie T, Zaidi H. Effect of respiratory motion on internal radiation dosimetry. *Med Phys*. 2014;41:112506.

ClearCheck

One-click plan evaluation

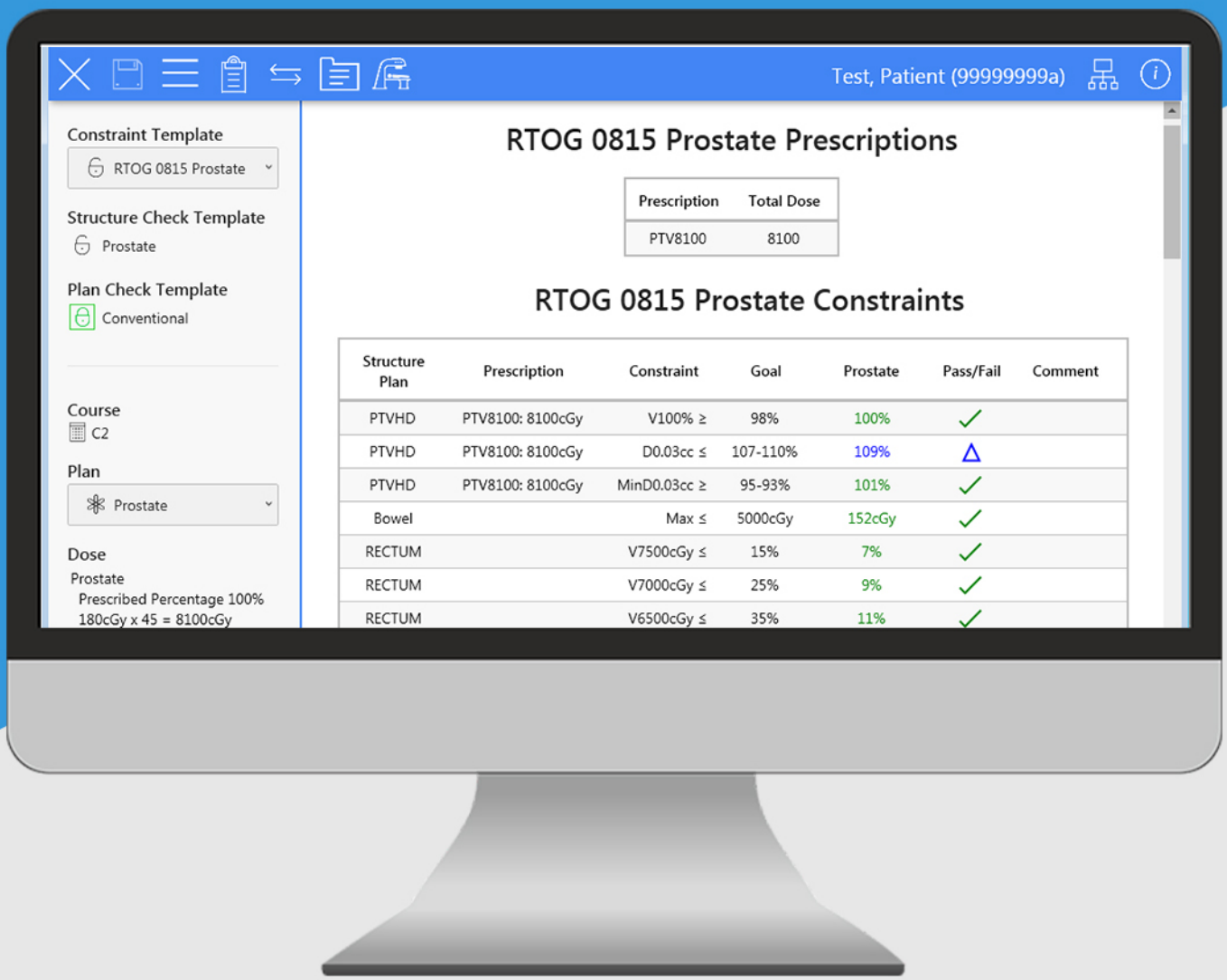

Dose Constraints ◦ Plan Checks

Structure Checks ◦ Collision Checks

RADformation.com